NASA
Technical
Paper
2865

February 1989

Raman Intensity as a Probe of Concentration Near a Crystal Growing in Solution

R. Allen Wilkinson

NASA

NASA Technical Paper 2865

1989

Raman Intensity as a Probe of Concentration Near a Crystal Growing in Solution

R. Allen Wilkinson
Lewis Research Center
Cleveland, Ohio

NASA
National Aeronautics and Space Administration
Office of Management
Scientific and Technical Information Division

Summary

This report presents the feasibility of using Raman spectral scattering signals for measurements of concentration profiles near a crystal interface during growth or dissolution. With KH_2PO_4 (KDP) as a test material, optical multichannel analyzer (OMA) detection of a solute Raman vibrational band provided direct quantification of solute concentration with band intensity. The intersection of incident laser and Raman collection optics provided three-dimensionally selective point measurements of the solution concentration field. Unlike many other techniques, the Raman band intensity is not sensitive to the typical temperature variations.

Precision calibration of Raman intensity versus KDP concentration with less than 1-percent standard deviation error levels was demonstrated. A fiber optic, which sampled incident laser intensity and coupled it to the OMA, provided a fully synchronized monitor of fluctuations in laser power to correlate with observed Raman signals. With 1 W of laser power at the sample, good data statistics required eight repeated data collections at approximately 2.5 min/collection. The accumulated time represents the concentration measurement time at one spatial location. Photomicroscopy documented a 30-μm-diameter by 200-μm-long laser Raman scattering region in the solution near the crystal surface. The laser beam was able to approach up to 25 μm from the crystal surface. However, a crystal surface reflected intensity contribution was weakly detectable. Nucleated microcrystals were seen in the crystal-growing solution. These microcrystals convect right up to the crystal surface and indicate no quiet diffusion region under normal gravity conditions. Translation of the solution cell with respect to the optics caused systematic intensity errors.

Introduction

An underlying need in the fundamental understanding of solution crystal growth is an experimental characterization of the concentration field in the vicinity of the crystal surface (refs. 1 to 5). Most crystal growth analyses postulate the concentration field (refs. 6 to 8). The concentration field is an important determinant of crystal growth morphology, defects, rate, and terminal size (refs. 9 to 11). In diffusion limited growth systems, a goal in low gravity, much effort has gone into trying to measure the concentration field (refs. 12 to 15).

This report presents a ground-based effort to explore the feasibility of employing Raman spectroscopy to quantify concentration near a crystal growing or dissolving in solution. Some attractive features of this measurement technique are the following: (1) the Raman intensity is an explicit linear function of the number of scattering species in the sampled volume, (2) three-dimensional resolution is possible because of the intersection of incident and collection optics, and (3) there is such weak temperature dependence that it is not perceptible over the 5 °C temperature range of interest. The measurements do require sequential spatial point measurements because of the three-dimensional resolution of the optical configuration.

Most measurements done previously are full-field (i.e., sample a spatial domain of macroscopic size). These techniques generally depend on the concentration (C) dependent optical index of refraction (n) variations in the solution (e.g., schlieren (refs. 1 and 16), differential, and holographic interferometry (refs. 17 and 18), and Moiré fringes (ref. 19)). Several problems of these techniques are revealed by the following relationship, which is the basis for the techniques:

$$\frac{\partial n}{\partial z} = \frac{\partial n}{\partial \rho}\frac{\partial \rho}{\partial z} \neq 0$$

where

$$\rho = \rho(C(\mathbf{r}),\ T(\mathbf{r}))$$

and ρ is the number density, z the distance normal to the crystal surface, $\mathbf{r}$ the three-dimensional position, and T the temperature. One problem is the implicit dependence of the index of refraction on concentration, which adds difficulty of analysis and uncertainties to the precision of the results. Also, the number density is roughly as sensitive to temperature as to concentration, again adding difficulty to the analysis. A further limitation is that variations of ρ tangential to the surface are integrated out by these techniques. That is, the observed refraction effects are a cumulative result of ρ variations along the entire optical path through the solution. A final problem is that the literature appears vague on its specification of concentration versus position resolution (refs. 1, 11, and 16 to 19).

This report contains a brief background on laser Raman spectroscopy, a description of the details of the experimental equipment and method, a discussion of the data collected and measurement precision, and the immediate conclusions drawn. Limitations discovered in applying the technique are also presented. The highlighting of these limitations is not to discourage users, but to aid the credible application of this technique. Lastly, a summary is provided with the overall conclusions on the feasibility of employing Raman scattering as a concentration probe near a crystal in solution.

Laser Raman Spectroscopy

The simplest picture of the technique is that of an intense (usually visible) monochromatic light beam impinging on a sample, and the sample weakly radiating a distribution of colored light in all directions. If the scattered light has a higher frequency than the laser, then it is called anti-Stokes Raman scattering. This study concentrated only on the scattered light of lower frequency than the laser, which is called Stokes Raman scattering. The essential dependences are reflected in the following relationship:

$$I_R \propto I_o N \tilde{\nu}_s^4 \alpha^2 \left[n(\tilde{\nu},T) + 1 \right]$$

where I_R is the scattered Raman intensity, I_o the incident laser intensity, N the number of molecules in the scattering volume, $\tilde{\nu}_s$ the frequency of the scattered light, n the Bose-Einstein distribution function which yields the temperature response, and α the molecular polarizability. The explicit linear dependence on N makes the intensity-to-concentration analysis simpler than the other methods cited in the introduction. The α gives rise to a spectrum for the scattered light with characteristic peaks. The 880 cm^{-1} peak of the phosphate ion in solution was chosen as the I_R source because it was isolated from other peaks and the strongest in the spectrum. The I_R was measured by taking the net integrated area under the peak of choice.

The laboratory instrumentation used here is pictured in figure 1 and includes (1) a laser, (2) a sample mount and scattered light collection optics on the optical rail on the nearest corner of the vibration damping table, (3) a spectrometer (or monochromator) in the large box on the table, which filtered the frequency of the scattered light recorded, and (4) a cooled optical multichannel detector in the casing appended vertically from the top of the spectrometer, which acted like a fast electronic photographic plate recorder of the frequency window passed by the spectrometer. Also shown are two computers used to record and manipulate spectral data.

The apparatus used was sufficient for this study, but was not an optimal design as will become apparent. Future activity needs to address optimization.

Experiment Description

The overall experimental method involved (1) establishing spatial resolution of the point measurements, (2) calibrating the linearity of collected Raman intensity with concentration standards, and (3) collecting Raman signals as a function of position near a growing or dissolving crystal in solution. Two essential activities, sample preparation and data analysis, supported this method. The key equipment functions were thermal control of the sample, illumination of the sample and frequency dispersion of collected light from the sample, and detection and recording of the dispersed light. The materials of choice were reagent grade KH_2PO_4 (KDP) for the crystal and solute, and deionized water for the solvent. Considerations in that choice were ease of crystal growth near room temperature, sufficient literature on the technique of growth, and optical transparency of the aqueous solutions so that laser intensity in the scattering volume was constant and measurable.

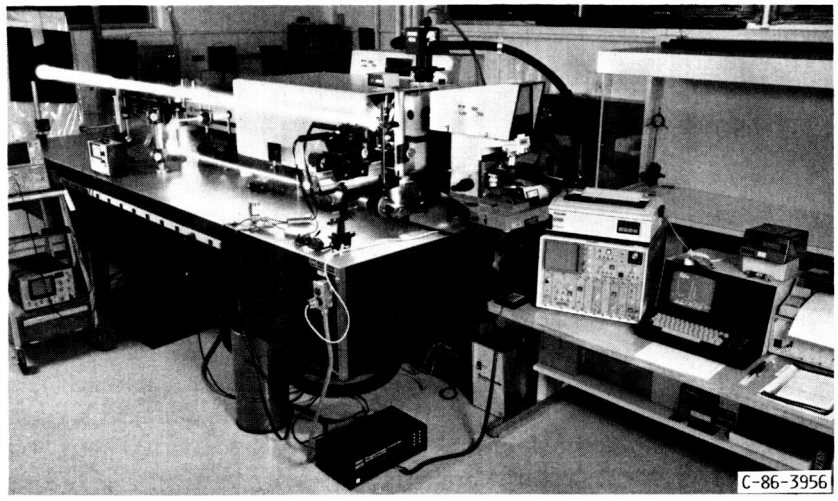

Figure 1.—Raman spectroscopy laboratory equipment.

Equipment

Spectrophotometric quartz cuvettes contained the solute and provided optically uniform and orthogonal windows. Solute temperature was thermostated by thermofoil heaters lining the walls and could be feedback-controlled to 0.1 °C. This is represented by the thermostat bath in figure 2. The crystal seed was grown on a brass screw threaded up to its head into a copper bar (the cold finger). The copper bar was also thermoelectrically temperature-controlled to 0.1 °C. A thermistor located 5 to 8 mm from the crystal, inside the copper bar, was used to record the crystal temperature. Linearized thermistors with readouts provided the data on both solute and crystal substrate temperatures. The portion of the copper bar submerged in solution was sealed and insulated with four layers of heat-shrinkable Teflon tube and some trapped air. Sealing was not perfect around the screw head.

The illumination source for the sample was an intensity-stabilized argon ion laser, which could provide 3 W of 5145 Å wavelength light. The light was beam-expanded, double-dispersed through Pellin-Broca prisms, and spatial-filtered to remove plasma lines. Upon steering the beam to the sample, approximately 1 W of light polarized perpendicular to the scattering plane was focused by a 75-mm-focal-length objective lens to a 30-μm-diameter beam waist at the scattering volume.

Scattered light was collected by an effective *f*/2.2 achromatic lens with its optical axis at 90° to the incident laser beam direction. The working distance to the lens was roughly 9 cm. All polarizations of scattered light passed into an *f*/8, 1-m-focal-length, double-dispersion spectrometer. The 2.43 Å/mm dispersion was more than needed, but the spectrometer's stray light rejection was beneficial. The *f*/number ratio reflects the ≈ 3.6X magnification of the object by the collection optics.

The spectrometer's entrance slit was set at 300 μm. The slit had a triangular mask that slid perpendicular to the slit orientation in order to field-stop the image of the scattering sample volume. An alignment periscope allowed backviewing through the entrance slit and collection optics. To test the field of view seen by the spectrometer one could locate a 200-μm pinhole where the scattering sample volume would be, focus its image on the entrance slit, and use a stereomicroscope to view the sample volume field through the periscope as the slit and triangular mask closed down and stopped off the field. The final view showed a trapezoidal aperture, the base of which spanned the 200-μm pinhole but cut off the top and bottom portions of the pinhole. The image was too fuzzy to photograph because of diffraction blur of the polychromatic light illuminating the pinhole. A better designed mask could have tightened the 200 μm dimension more, but signal would be lost with the smaller field stop. Finally, the 30-μm-diameter incident laser beam waist, when imaged through the ≈ 3.6X magnifying collection optics, safely fit within the 300-μm slit width field stop. This then established the 200-μm-long by 30-μm-diameter cylindrical volume that scattered light into the spectrometer.

In the spectrometer there were 11 reflections between entrance and exit slits. To get a measure of light thoroughput efficiency for a selected passband frequency window, one must consider what fraction of input light is left after 11 repeated reflections. Assuming 95 percent reflectivity for each reflector, one gets $(0.95)^{11} = 0.57$, or 57 percent throughput.

The light throughput of the spectrometer was collected by a 1024-element microchannel plate intensified diode array with thermoelectric cooling to -30 ± 0.1 °C. Each photodiode spanned a 25-μm spatial width. This was the detector for the optical multichannel analyzer (OMA) system. The 880 cm^{-1}

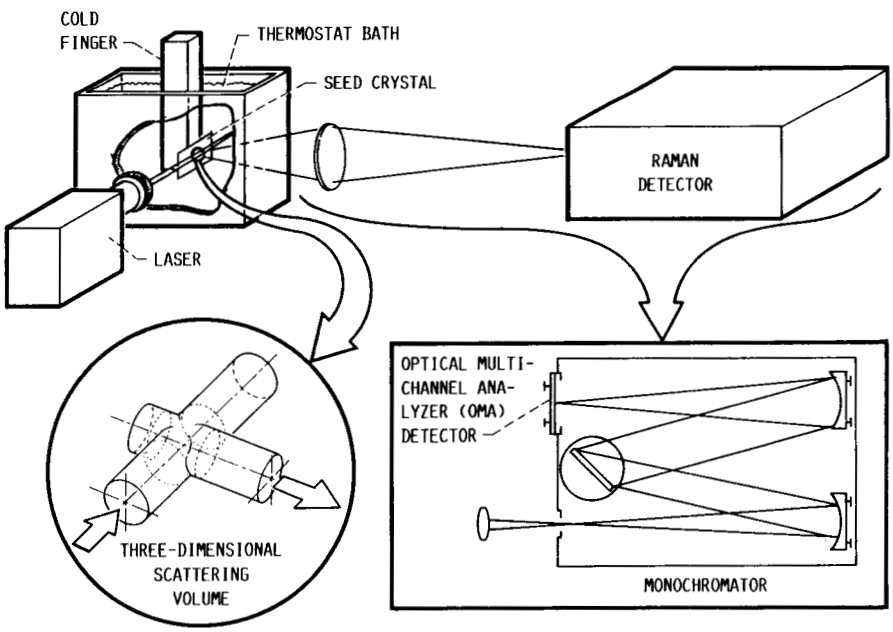

Figure 2.—Schematic representation of Raman experimental configuration.

peak of the phosphate ion in solution fit readily into the frequency window passed by the spectrometer. That frequency window left about 200 channels on each end of the diode array unused. Figure 3 shows what a collector spectrum looked like.

A fiber optic was mounted to illuminate one of the two unused portions of the diode array (fig. 3). The source of light for the fiber optic was incident laser light scattered from a Pellin-Broca prism mount. The collection cone for the fiber was defined to exclude any other sources. The source had to be on the laser end of the plasma line spatial filter to avoid variable back reflections from the sample cell contributing to the light picked up by the fiber. The fiber optic thus provided a synchronized sampling of incident laser light recorded together with Raman scattered light. Later, in the Data Analysis subsection, while establishing the precision of the scattered intensity data, it will be clearer why the fiber optic was valuable.

The OMA accumulated counts in each diode element for a user-selected period of time and then read and stored the array of data digitally in memory. Repetitive accumulate and store operations built up a spectrum displayed on a computer screen. This signal-averaged spectrum could be manipulated and/or stored to floppy diskette. Only raw counts were stored. Instrumental dark and background counts were not subtracted. This reduced the sources of statistical fluctuations in the data analyzed.

Sample Preparation

Two types of samples were needed: concentration calibration standards and crystal-growing solutions with seed crystals. Five standard concentrations were each prepared in 1000.0 ± 0.5 ml (0.05 percent error) calibrated volumetric flasks at 20 °C with American Chemical Society (ACS) reagent grade KDP and thermally equilibrated 18.3-MΩ deionized water. The gram molecular weight of KDP was taken as 136.09 g/mole. The following samples were weighed out and dissolved in a flask:

1.50 M ⇒ 204.14 ± 0.04 g (0.02 percent error)
⇒ 1.5000 M ± 0.07 percent

1.48 M ⇒ 201.41 ± 0.04 g (0.02 percent error)
⇒ 1.4800 M ± 0.07 percent

1.25 M ⇒ 170.12 ± 0.08 g (0.05 percent error)
⇒ 1.250 M ± 0.10 percent

1.00 M ⇒ 136.09 ± 0.04 g (0.03 percent error)
⇒ 1.0000 M ± 0.08 percent

0.75 M ⇒ 102.07 ± 0.09 g (0.09 percent error)
⇒ 0.750 M ± 0.14 percent

Heats of solution and volume change on dissolution were

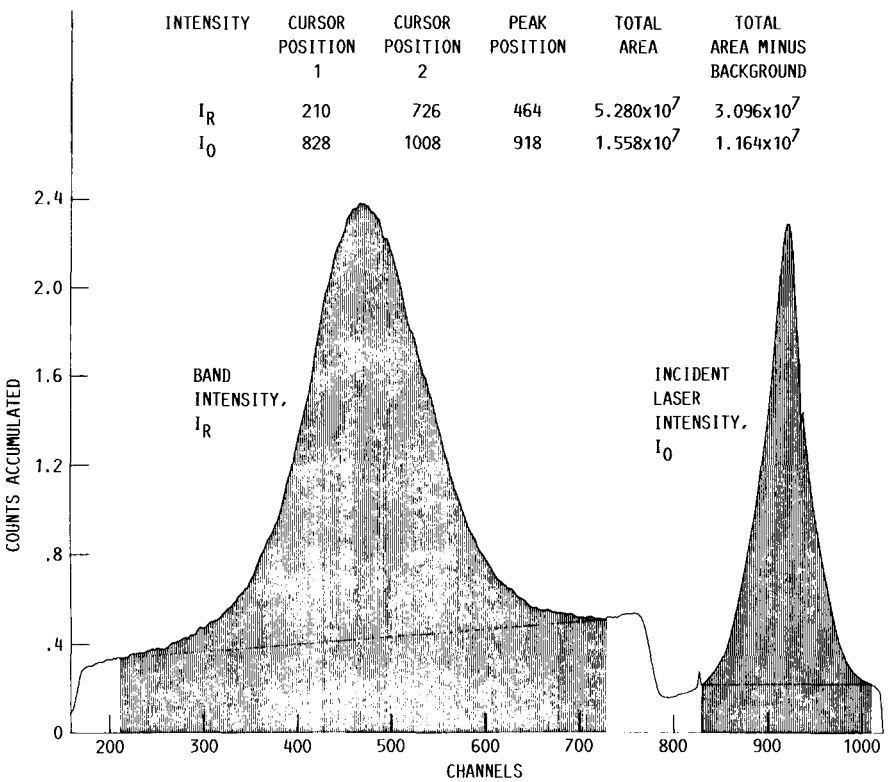

Figure 3.—Example of stored OMA data file (1.48 M KDP) with prenormalization integrated intensities shown (cursor position indicated by channel number, area measured in counts).

accommodated by equilibrating solutions for a day before topping off flasks with the last few milliliters of water. The precision of these concentration standards were two to ten times better than the intensity precision achieved in this study.

Seed crystals were produced by submerging the chilled (≈ 15 °C) copper cold finger in a beaker of 1.5 M solution and letting the crystal develop for a couple of days on the brass screw. The 1.5 M solution worked well as the crystal-growing solution here and for the solution crystal growth Raman concentration measurements because, at 20 °C, 1.5 M is close to the saturation concentration.

Data Analysis

Concentration calibration data sets consisted of four or eight data files. A data file (fig. 3) was a signal-averaged spectrum typically requiring 2.5 min to accumulate. A file possessed two peaks: one for the 880 cm^{-1} phosphate vibrational band I_R and one for the fiber optic sampled incident laser intensity I_o. An intensity was calculated by taking the net integral, either 518 channels for the phosphate band or 182 channels for I_o, under a peak.

Within a data set, I_R and I_o were averaged to yield $\bar{I}_R$ and $\bar{I}_o$ with their respective standard deviations σ_R and σ_o. If $\sigma_o > \sigma_R$, then the data set was discarded because there are more sources of noise for I_R than for I_o, and to observe $\sigma_o > \sigma_R$ would be coincidental and not a reflection of the true uncertainties. Also, σ_o was required to be less than 0.5 percent (except in the 0.75 M case where less effort was spent) in order to achieve a $\sigma_R < 0.5$ percent. This was an arbitrary choice in trying to push the limits of precision of the Raman study. This procedure provided a quality check on a sequence of data files collected in close time proximity on identical samples and optics. Data files were then collected on several different sample-and-optics setups over a period of several days.

Ultimately each data file of I_R was normalized to a per-second basis, divided by the incident intensity (close to 1 W) as measured by a photometer, and presented as a data point in figure 4. The I_o measured with the fiber optic was not used to normalize the data because a variable neutral density filter was used daily to adjust the I_o detected to optimize its recording within the dynamic range of the OMA and thereby achieve the best signal-to-noise ratio possible. In the normalization of I_R no error was assigned to the integration time or the incident intensity. The integration time was an integral number of clock cycles of the OMA's computer. The error was not likely to be detectable. It was difficult to characterize the effective uncertainty in the photometer measurement over the integration time of a data set. Therefore, no uncertainty was assigned to it. However, since $\sigma_o < 0.5$ percent, a number read from the photometer during signal collection should be useful.

The next section will discuss how the intensity-versus-concentration plot was analyzed and will present observations on the Raman signals acquired during in situ crystal growth or dissolution.

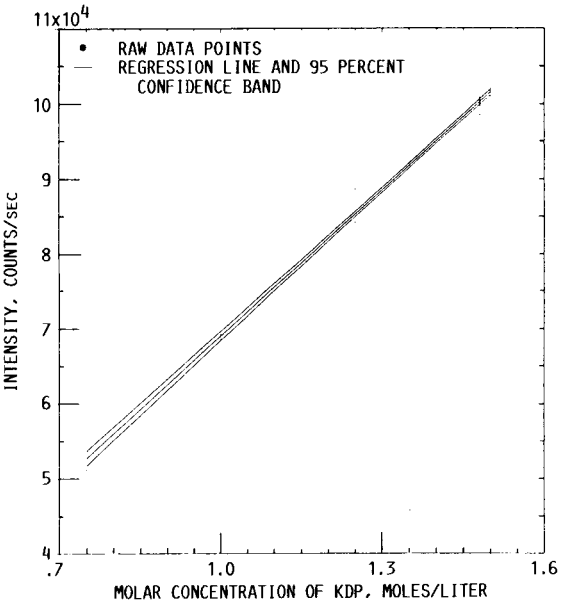

Figure 4.—Calibration curve of normalized intensity of Raman scattering versus solution concentration.

Results and Discussion

A plot of Raman intensity versus standard concentrations is presented in figure 4. Table I shows the raw data points at the five standard concentrations used in figure 4. The higher density of points at larger concentrations reflects the expectation that the actual crystal-growing experimental data would be in that domain. The data also represent several different days of experimental operation with different samples, cuvettes, and optical alignment. This is intended as a worst case scenario of data spread.

Given the data, a linear least-squares fit was executed together with calculation of the 95 percent confidence interval. The curves allow one to describe the expected concentration and its uncertainty for a measured data set's average I_R. If one looks at the expected concentration uncertainty in the 1.45 to 1.50 M region, one finds a ≤ 1 percent uncertainty. Hence, a data set from a point concentration measurement consisting of eight data files that takes approximately 20 min to acquire and that yields an I_R with a $\sigma_R \leq 0.5$ percent can be related to an expected concentration with ≤ 1 percent uncertainty.

Figure 4 shows intensity data sets with averages outside of the confidence band. This may be due to poorness of intensity normalization via the photometer. However, the statistical analysis of the fit showed an excellent fit.

In the Equipment subsection of the preceding section, the spatial resolution of a concentration point measurement was established as a 30-μm-diameter by 200-μm-long cylindrical volume. Both dimensions can be reduced; the diameter by a

TABLE I.—INTENSITY AND CONCENTRATION DATA USED TO CONSTRUCT FIGURE 4

Concentration, moles/liter	Intensity, counts/sec	Concentration, moles/liter	Intensity, counts/sec
0.75	0.5113219×10^5	1.48	1.005738×10^5
	.5072228		1.012393
	.5110880		1.004257
	.5130135		1.008222
1.00	0.6925959×10^5		1.004897
	.6904734		.9998617
	.6909921		1.011488
	.6895987		1.007680
	.6895911		1.002187
	.6926015		.9879690
	.6891606		.9783628
	.6859310		.9763970
1.25	0.8380996×10^5		.9844650
	.8415667		.9854216
	.8431658		.9895809
	.8407888		.9810309
	.8792191		.9863370
	.8861900	1.50	1.010750×10^5
	.8871991		1.008708
	.8851799		1.002516
	.8872025		1.015930
	.8757249		1.027254
	.8827858		1.017187
	.8829141		1.018542
1.48	1.008730×10^5		1.013812
	1.011147		1.009466
	.9998883		1.011423
	.9982295		1.010128
	1.001651		1.014471
	.9977448		1.003135
	1.007724		1.011106
	.9974744		1.016819
	1.001458		1.024370
	.9964356		1.020641
	1.001922		1.017917
			1.020541
			1.016699

shorter focal length incident laser focusing lens and/or by a larger diameter laser beam incident on the focusing lens, and the length by using an adjustable slit in place of the sliding triangular mask at the spectrometer entrance slit. A reduced scattering volume would mean a less detectable signal, with the signal scaling as the size of the scattering volume. To maintain the data precision and data collection times represented in this report one would have to scale up the incident laser intensity as the reciprocal volume. There is an upper bound on laser intensity, though, because of the onset of nonlinear Raman scattering or sample heating if optical absorption is present in the solution.

With the baseline performance characterization for the feasibility study completed, data were collected from solution near a growing or dissolving crystal. Upon collecting Raman data, several difficulties arose. The main problem was the lack of a quiet diffusion depletion layer near the surface. Since crystal growth (dissolution) was induced by cooling (warming) the seed crystal 3 °C with respect to the nearly saturated solution at 20 °C, a buoyancy-driven convection of solution was visible right up to the crystal surface. This was made apparent by microcrystals floating in the nearly saturated solution and viewed through the stereomicroscope with better than 10-μm resolution. Growth or dissolution was clearly happening in these situations because 24 hr of waiting showed significant crystal size change.

The microcrystals never seemed to be preventable in these nearly saturated solutions. Careful filtering and clean glassware never completely eliminated microcrystals.

By setting up crystal dissolution in an isothermal seed and solution system, convection could be eliminated. The solution was slightly below saturation then (by ≈ 0.05 M). If it was far below saturation (by ≈ 0.25 M), then the concentration gradient near the crystal refracted the incident laser beam such that the scattering sample volume detected was not predictable. This constraint of weak undersaturation explains why precision of intensity-versus-concentration calibration was pushed. Also some crystal-growing systems have only small concentration changes in the solution in the diffusion depletion layer (refs. 7 and 11).

It was in the isothermal dissolution system that other difficulties were characterizable. These included focal length changes of the Raman collection and incident laser focusing optics upon translation of the solution sample along either of the respective optical axes. Also a weakly detectable Raman intensity was reflected from the crystal surface increasingly as the scattering sample volume moved closer to the crystal surface. One could approach the surface up to 25 μm with the laser beam without the $1/e^2$ gaussian beam profile tails introducing Raman scattering from the solid KDP.

Analysis of Limitations

Discussions of the focal length changes and surface-reflected Raman intensity difficulties just described are presented in this section. It should be emphasized that these limitations are a consequence of the experimental system used. Adaptations to improve performance are suggested at the end of this section. Also, the lack of temperature sensitivity is analyzed here.

Focal length changes were analyzed with geometrical optics. The focal length change of a lens in air collecting light from an object inside the KDP solution was calculated as a function of translations of the interface of solution and air, several geometric parameters, and the indices of refraction.

Given a fixed distance from the collection lens to the spectrometer entrance slit and a fixed focal length for the lens, then a fixed object distance o in air is determined. Let the lens have an aperture stop of radius r, and the object have a height h. For generality let the air and KDP solution have indices of refraction n_b and n_a, respectively. Finally, let b equal the lens-to-solution/air interface, and a equal the solution/air

interface-to-object distances. Then using Snell's law, one derives the following focal length change with respect to o:

$$a + b - o = (o - b)\left[\frac{r-h}{o}\sqrt{\frac{o^2 n_a^2}{(r-h)^2 n_b^2} + \frac{n_a^2}{n_b^2} - 1} - 1\right]$$

The focal length change is a linear function of b. From figure 5, a 100-μm translation along either of the orthogonal optical axes will lead to an $\approx$36-μm shift in the focal plane. Hence, if the cell containing the solution and crystal sample is translated with respect to fixed laser focusing and Raman collection optics, a nonnegligible misalignment of the optics will arise and the collected signal will decrease. That leaves translations of the cell perpendicular to the scattering plane available for pointwise mapping. As a result, for a given orthogonal optical alignment the activity reported here can reasonably map out a 200-μm-thick by 30-μm-wide line in front of the crystal.

Next, Raman intensity reflected from the crystal surface was weakly detectable when the crystal surface normal was in the scattering plane; when oriented orthogonal to the scattering plane, no problem existed. Rayleigh scattered intensity was used to visualize the effect since the Raman intensity was too weak. Figure 6 shows a photograph of Rayleigh intensity scattered from a ground glass surface 50 μm away from the laser beam. The OMA Raman detector did show a 0.4-percent intensity enhancement 40 μm from the surface compared with 3 mm from the surface. Although less than the σ_R, it was universally reproducible.

OPTICS	APERTURE RADIUS, r, CM	HEIGHT, h, CM	OBJECT DISTANCE, o, CM
——— COLLECTION	2.2	0.002	9.0
— — — INCIDENT LASER	0.5	0.002	7.5

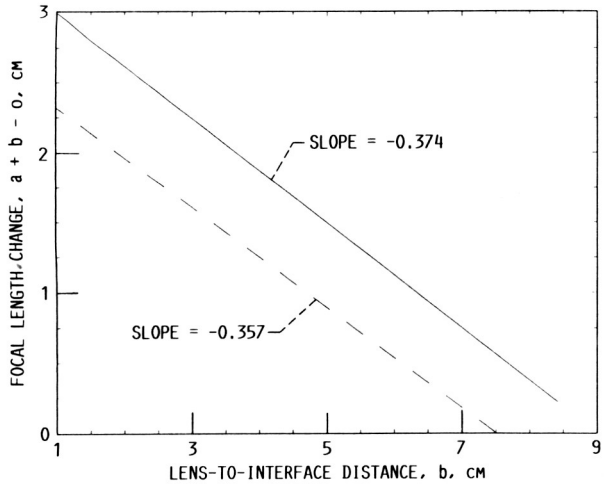

Figure 5.—Change in focal length of collection and incident laser optics due to cell translation along either optical axis (KDP solution and air indices of refraction n_a and n_b, 1.356 and 1.00, respectively).

To further characterize this observation, a calculation was performed, again with geometrical optics. The question was how much light could get into the collection cone if it originated beyond the focal plane? A source (see fig. 7) was located at the focal plane a distance o from the lens of aperture radius r and radiated I_o into the collection optics. It was assumed that an equal I_o impinged on a diffusely reflecting flat plane a distance d behind the focal plane (away from the collection optics). Further, this resulted in a uniform light source on the reflecting plane of linear extent S equal to the spectrometer entrance slit height divided by the collection optics magnification (300 μm/3.6X). In effect, S was the slit image size at the object plane. If a ray from the reflecting plane did not pass through the slit image, then it would not be collected by the spectrometer. Also, if a ray had an angle with respect to the optical axis greater than that defined by the collection cone, whether it passed through the slit image or not, then it would not be collected.

These criteria gave rise to two functional regimes for the intensity collected. The two regimes were demarcated by a

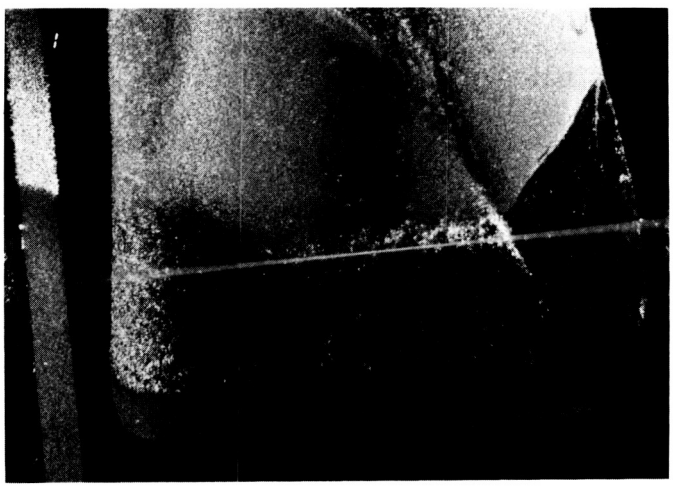

Figure 6.—Laser light scattering and surface reflection of scattered light.

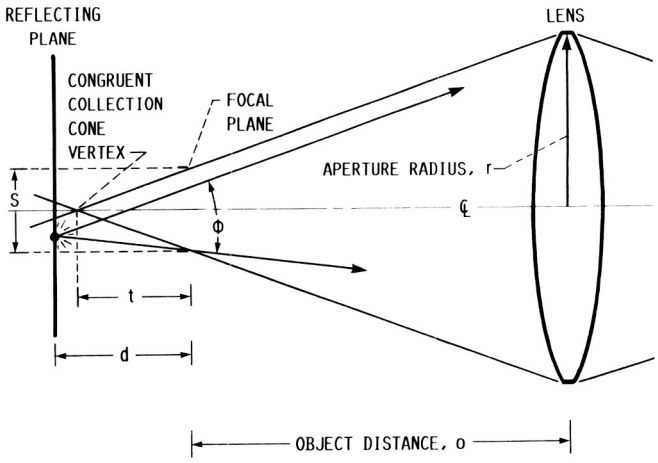

Figure 7.—Geometrical optics schematic used in analysis of crystal surface reflected Raman (ϕ indicates collection angle permitted and shows cone ange and slit limitations on collectible rays).

distance t beyond the focal plane, which was at the vertex of a cone with an angle congruent to the collection cone but intersecting the limit points of the image slit; that is, $\frac{1}{2}\ S/t = r/o$ by congruent angles, or $t = So/2r$.

Each point on the reflecting plane was defined to radiate with angular uniformity (diffuse reflector) and $R(I_o/S)$ strength, where R is the reflectivity at normal incidence due to the index of refraction mismatch between crystalline and solution KDP (1.51 and 1.356, respectively). A small angle approximation ($\tan\theta \cong \theta$) was used to transform the collection angle permitted for each point source on the reflecting plane into the spatial variables of integration. A one-dimensional integration over S was performed with the following results:

$$\frac{I}{I_o} = 1 + R - \frac{Rdr}{2So} \qquad \text{for } 0 \leq d \leq 2t$$

$$= 1 + \frac{RSo}{2rd} \qquad \text{for } 2t \leq d \leq \infty$$

Figure 8 shows a plot of these results for $o = 9.0$ cm and $R = 2.89 \times 10^{-3}$. The two regimes match up smoothly with $t = 175$ μm for $r = 2.2$ cm and $t = 276$ μm for $r = 1.4$ cm. Stopping down the aperture leads to longer range and stronger reflection contributions. When the crystal surface is at $d = 0$, then RI_o is added to the intensity. The reflection has a very long-range contribution. The experimentally observed contribution of 0.4 percent is in agreement with the 0.2 to 0.3 percent calculated here given the uncertainties of the real reflectivity in the experiment. The conclusion is that a small but characterizable intensity artifact arises when the crystal surface normal is in the scattering plane.

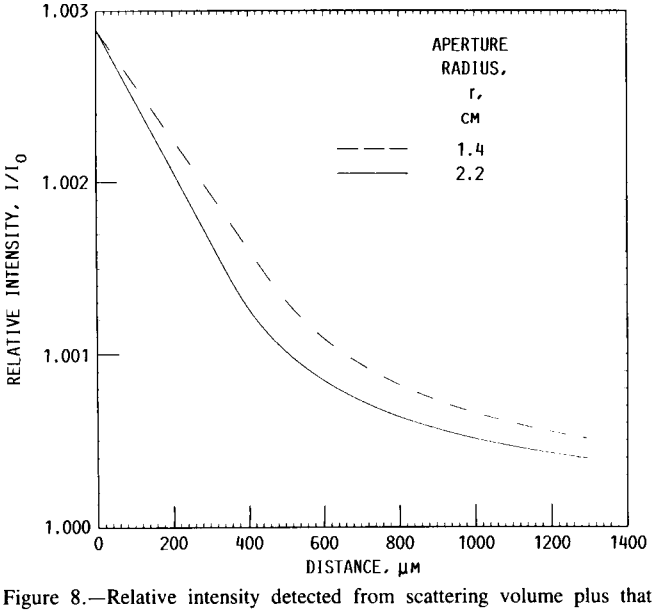

Figure 8.—Relative intensity detected from scattering volume plus that reflected from crystal surface for two different collection lens apertures (distance measured from crystal surface).

Finally, the temperature sensitivity of the Stokes Raman intensity was examined. Stokes Raman intensity has a temperature dependence via the Bose-Einstein distribution function for vibrational quanta of

$$\frac{1}{1 - \exp\left(\frac{-hc\tilde{\nu}}{k_B T}\right)} \tag{1}$$

where h is Planck's constant, c is the speed of light, k_B is Boltzmann's constant, $\tilde{\nu}$ is the relative frequency location of the Raman peak in cm^{-1}, and T is the absolute temperature in kelvin. To get the relative intesity change with respect to temperature, one differentiates (1) and divides the result by (1), getting

$$\frac{1}{\exp\left(\frac{hc\tilde{\nu}}{k_B T}\right) - 1} \left(\frac{hc\tilde{\nu}}{k_B T^2}\right) \tag{2}$$

Thus, the sensitivity at 293 K, roughly lab conditions for this report, and at 880 cm^{-1} is 0.02 percent/K. That is at least an order of magnitude below detectability, and it confirms that no effect will be seen over a 1 to 5 °C temperature range.

For information, at 293 K and 425 cm^{-1}, the sensitivity is 0.10 percent/K. This reflects a strong frequency dependence. One should keep this in mind if a Raman peak at a different frequency were to be studied.

To conclude this section, temperature does not complicate the interpretation in this technique, and Raman intensity reflected from the crystal surface does not add artifact intensity to that recorded when the crystal surface normal is oriented orthogonal to the scattering plane. Thus, some limitations can easily be resolved. The other limitation discussed is really a matter of user choice. One can choose to map out either a line or a plane near a crystal, where an orthogonal optics configuration provides a line and Raman backscatter configuration provides a plane.

Concluding Remarks

This report presents the feasibility of using Raman spectral scattering signals for measurements of concentration profiles near a crystal interface during growth or dissolution. Optical multichannel analyzer (OMA) detection of a solute vibrational band of KH_2PO_4 (KDP) was shown to provide direct quantification of solute concentration with band intensity. The intersection of incident laser and Raman collection optics provided three-dimensionally selective point measurements of the solution concentration field. The Raman band intensity was shown not to be sensitive to the typical temperature variations encountered in this study.

Precision calibration of Raman intensity versus KDP concentration with less than 1 percent standard deviation error levels was demonstrated. A fiber optic, which sampled incident laser intensity and coupled it to the OMA, provided a fully synchronized monitor of fluctuations in laser power to correlate with observed Raman signals. With 1 W of laser power at the sample, good data statistics required eight repeated data collections at approximately 2.5 min/collection. The accumulated time represents the concentration measurement time at one spatial location. Greater spectrometer efficiency, higher detector sensitivity, and increased incident laser intensity are vehicles for reducing data collection time. Photomicroscopy documented the 30-μm-diameter by 200-μm-long laser Raman scattering region in the solution near the crystal surface. The laser beam was able to approach up to 25 μm from the crystal surface. However, a crystal surface reflected intensity contribution was weakly detected and analytically calculated. Nucleated microcrystals were seen in the crystal-growing solution. These microcrystals convect right up to the crystal surface and indicate no quiet diffusion region for thermally driven crystal growth under normal gravity conditions. Translation of the solution cell with respect to the optics caused systematic intensity errors. A calculated change of the focal length as a function of translation was given.

To map out a line in the solution pointwise, an orthogonal optical setup suffices, but the best that can be done is to map out a plane pointwise by using a backscattering optical configuration with the crystal surface normal orthogonal to the Raman optical axis. This observation about backscattering is an inference from this study and was not actually tested. Fiber optic collection and illumination optics could in principle remove this constraint and permit full three-dimensional spatial mapping.

Since this is a new approach to concentration measurements in crystal-growing work, more practitioners are needed to pass judgement on its durable merits.

Lewis Research Center
National Aeronautics and Space Administration
Cleveland, Ohio, November 29, 1988

References

1. Tsukamoto, K.: In-situ Observation of Mono-Molecular Growth Steps on Aqueous Solution Grown Crystals and the Transport of Molecules to the Crystals. The 1986 Get Away Special Experimenter's Symposium, L.R. Thomas and F.L. Mosier, eds., NASA CP-2438, 1987, pp. 233-238
2. Torgesen, J.L.; Horton, A.T.; and Saylor, C.P.: Equipment for Single Crystal Growth from Aqueous Solution. J. Res. Nat. Bur. Stand—C. Eng. Instrum., vol. 67C, no. 1, Jan.-Mar., 1963, pp. 25-32.
3. Ginzburg, V.M.; Guseva, I.N.; and Kramarenko, V.A.: Distribution of Concentration in a Solution During Growth of Potassium Dihydrogen Phosphate Single Crystals. Gologr. Metody i Apparatura, Primenyaemaya v Fiz. Issled, 1974, pp. 51-54 (in Russian).
4. Prieto, M.; and Amoros, J.L.: On the Influence of Hydrodynamic Environment on Crystal Growth. Bull. Mineral., vol. 104, no. 2-3, 1981, pp. 114-119.
5. Uhran, M.L.; Holland, L.R.; and Wear, W.O.: Accommodation Requirements for Microgravity Science and Applications Research on Space Station. (JN67801, Wyle Labs Inc.; NASA Contract NAS3-24654) NASA CR-175038, 1985, pp. A51-A58.
6. Robertson, D.S.: A Study of the Growth and Growth Mechanism of Potassium Dihydrogen Orthophosphate Crystals from Aqueous Solution. J. Mater. Sci., vol. 16, no. 2, Feb. 1981, pp. 413-421.
7. Zundelevich, Y.: Chemical Engineering Principles of Constant Temperature—Constant Supersaturation Growth of Potassium Dihydrogen Phosphate (KDP) Crystals. UCID-20155, Aug. 1984.
8. Copper J.F.; and Singleton, M.F.: Rapid Growth of Potassium Dihydrogen Phosphate Crystals. UCRL-91795, Jan. 1985.
9. Belouet, C.: Growth and Characterization of Single Crystals of the KDP Family. Prog. Cryst. Growth Charact., vol. 3, no. 2-3, 1980, pp. 121-156.
10. Joshi, M.S.; and Paul, B.K.: Effect of Supersaturation and Fluid Shear on the Habit and Homegeneity of Potassium Dihydrogen Phosphate Crystals. J. Cryst. Growth, vol. 22, no. 4, 1974, pp. 321-327.
11. Robert, M.C.; and LeFaucheux, F.: Results and Development of Solution Growth Space Experiments. Proceedings of the 6th European Symposium on Material Sciences Under Microgravity Conditions, ESA SP-256, W.R. Burke, ed., European Space Agency, Paris, France, 1986, pp. 77-85.
12. Owen, R.B.; Kroes, R.L.; and Witherow, W.K.; Results and Further Experiments Using Spacelab Holography. Opt. Lett., vol. 11, no. 7, July 1986, pp. 407-409.
13. Lind, M.D.; and Nielson, K.F.: LDEF Experiments: Crystal Growth by a Solute Diffusion Process. Proceedings of the 4th European Symposium on Materials Sciences Under Microgravity, ESA SP-191, T.D. Guyenne and J. Hunt, eds., European Space Agency, Paris, France, 1983, pp. 167-174.
14. Lal, R.B.: The Study of Crystals for Space Processing and the Effect of 0-Gravity. (AAMU-NAS-002, Alabama Agricultural and Mechanical College; NASA Grant NSG-8033) NASA CR-149672, 1977.
15. Schmitt, G.: The G-002 JUFO-1 Payload: Its Objectives and Results. Get Away Special Experimenter's Symposium, C.R. Prouty, ed., NASA CP-2324, 1984, pp. 135-142.
16. Matuchova, M.; and Van Enckevort, W.J.P.: Observation of Concentration Fields Around Growing or Dissolving KDP Crystals by Using Schlieren Technique. Industrial Crystallization '84, S.J. Jancic and E.J. DeJong, eds., Elsevier, 1984, pp. 237-240.
17. Goldsztaub, S.; Itti, R.; and Mussard, F.: Role de la Diffusion dans la Croissance des Cristaux a Partir de Solutions. J. Cryst. Growth, vol. 6, no. 2, 1970, pp. 130-134.
18. Kern, R.: Facies of Several Ionic Crystals with Simple Structures. A. The Changes of Facies in a Pure Medium. Bull. Soc. Franc. Mineral. Crist., vol. 76, 1953, pp. 325-364.
19. Hirano, E.; and Ogawa, T.: Measurements of the Concentration Gradient Around a Growing Crystal in an Aqueous Solution by Moire Fringes. J. Cryst. Growth, vol. 51, no. 1, 1981, pp. 113-118.

NASA
National Aeronautics and Space Administration

Report Documentation Page

1. Report No.	2. Government Accession No.	3. Recipient's Catalog No.
NASA TP-2865		

4. Title and Subtitle	5. Report Date
Raman Intensity as a Probe of Concentration Near a Crystal Growing in Solution	February 1989
	6. Performing Organization Code

7. Author(s)	8. Performing Organization Report No.
R. Allen Wilkinson	E-4397
	10. Work Unit No. 674-24-05

9. Performing Organization Name and Address	11. Contract or Grant No.
National Aeronautics and Space Administration Lewis Research Center Cleveland, Ohio 44135-3191	
	13. Type of Report and Period Covered: Technical Paper

12. Sponsoring Agency Name and Address	14. Sponsoring Agency Code
National Aeronautics and Space Administration Washington, D.C. 20546-0001	

15. Supplementary Notes

16. Abstract

This report presents the feasibility of using Raman spectral scattering signals for measurements of concentration profiles near a crystal interface during growth or dissolution. With KH_2PO_4 (KDP) as a test material, optical multichannel analyzer (OMA) detection of a solute Raman vibrational band provided direct quantification of solute concentration with band intensity. The intersection of incident laser and Raman collection optics provided three-dimensionally selective point measurements of the solution concentration field. Unlike many other techniques, the Raman band intensity is not sensitive to the typical temperature variations. Precision calibration of Raman intensity versus KDP concentration with less than 1-percent standard deviation error levels was demonstrated. A fiber optic, which sampled incident laser intensity and coupled it to the OMA, provided a fully synchronized monitor of fluctuations in laser power to correlate with observed Raman signals. With 1 W of laser power at the sample, good data statistics required eight repeated data collections at approximately 2.5 min/collection. The accumulated time represents the concentration measurement time at one spatial location. Photomicroscopy documented a 30-μm-diameter by 200-μm-long laser Raman scattering region in the solution near the crystal surface. The laser beam was able to approach up to 25 μm from the crystal surface. However, a crystal surface reflected intensity contribution was weakly detectable. Nucleated microcrystals were seen in the crystal-growing solution. These microcrystals convect right up to the crystal surface and indicate no quiet diffusion region under normal gravity conditions. Translation of the solution cell with respect to the optics caused systematic intensity errors.

17. Key Words (Suggested by Author(s))	18. Distribution Statement
Solution crystal growth Concentration profiling Raman spectroscopy	Unclassified – Unlimited Subject Category 35

19. Security Classif. (of this report)	20. Security Classif. (of this page)	21. No of pages	22. Price*
Unclassified	Unclassified	13	A03

NASA FORM 1626 OCT 86

*For sale by the National Technical Information Service, Springfield, Virginia 22161

NASA-Langley, 198